Deep–Sea Research II 209 (2023) 105277

Contents lists available at ScienceDirect

Deep-Sea Research Part II

journal homepage: www.elsevier.com/locate/dsr2

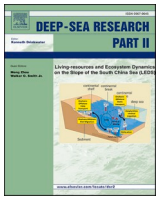

Vertical imbalance in organic carbon budgets is indicative of a missing vertical transfer during a phytoplankton bloom near South Georgia (COMICS)

S.L.C. Giering [a,*], R. Sanders [a], S. Blackbird [b], N. Briggs [a], F. Carvalho [a], H. East [a], B. Espinola [a], S.A. Henson [a], K. Kiriakoulakis [c], M.H. Iversen [d,e], R.S. Lampitt [a], K. Pabortsava [a], C. Pebody [a], K. Peel [a], C. Preece [b], K. Saw [a], M. Villa-Alfageme [f], G.A. Wolff [b]

[a] National Oceanography Centre, Southampton, SO14 3ZH, UK
[b] School of Environmental Sciences, University of Liverpool, Liverpool, L69 3GP, UK
[c] School of Biological and Environmental Sciences, Liverpool John Moores University, Liverpool, L3 3AF, UK
[d] Alfred Wegener Institute for Polar and Marine Research, Bremerhaven, 28570, Germany
[e] MARUM and University of Bremen, Bremen, 28359, Germany
[f] Dept. of Applied Physics II. ETSIE. universidad de Sevilla, Sevilla, 41012, Spain

ARTICLE INFO

Handling Editor: Prof. J Aristegui

Keywords:
Biological carbon pump
Sinking particles
Mesopelagic carbon budget
Southern Ocean
Non-steady state

ABSTRACT

The biological carbon pump, driven principally by the surface production of sinking organic matter and its subsequent remineralization to carbon dioxide (CO_2) in the deep ocean, maintains atmospheric CO_2 concentrations around 200 ppm lower than they would be if the ocean were abiotic. One important driver of the magnitude of this effect is the depth to which organic matter sinks before it is remineralised, a parameter we have limited confidence in measuring given the difficulty involved in balancing sources and sinks in the ocean's interior. One solution to this imbalance might be a temporal offset in which organic carbon accumulates in the mesopelagic zone (100–1000 m depth) early in the productive season before it is consumed later. Here, we develop a novel accounting method to address non-steady state conditions by estimating fluxes of particulate organic matter into, and accumulation within, distinct vertical layers in the mesopelagic zone using high-resolution spatiotemporal vertical profiles. We apply this approach to a time series of measurements made during the declining phase of a large diatom bloom in a low-circulation region of the Southern Ocean downstream of South Georgia. Our data show that the major export event led to a significant accumulation of organic matter in the upper mesopelagic zone (100–200 m depth) which declined over the following weeks, implying that temporal offsets need to be considered when compiling budgets. However, even when accounting for this accumulation, a mismatch in the vertically resolved organic carbon budget remained, implying that there are likely widespread processes that we do not yet understand that redistribute material vertically within the mesopelagic zone.

1. Introduction

Biological processes in the ocean play an important role in the global carbon cycle, exporting carbon from the ocean surface to the deep ocean, where it can be stored over long time scales. Without this process, called the 'biological carbon pump' (Giering and Humphreys, 2018; Volk and Hoffert, 1985), atmospheric CO_2 concentrations would be, according to models, 200 ppm higher than at present (Parekh et al., 2006). A key driver of the biological carbon pump is the formation of carbon-rich sinking particles, such as aggregated phytoplankton and detritus or faecal pellets, and their transport to the deep ocean, where they remain out of contact with the atmosphere. In the deep ocean, sinking particles typically undergo transformation and consumption, which alters their sinking velocity and organic matter content and ultimately reduces the particulate carbon flux (Martin et al., 1987). The most rapid reduction in particulate carbon flux occurs in the mesopelagic zone, the region between the bottom of the productive layer and 1000 m depth (Iversen et al., 2010; Stemmann et al., 2004). How much

* Corresponding author.
E-mail address: s.giering@noc.ac.uk (S.L.C. Giering).

https://doi.org/10.1016/j.dsr2.2023.105277
Received 29 September 2022; Received in revised form 17 February 2023; Accepted 6 March 2023
Available online 8 March 2023

and where exactly this reduction occurs determines how long the carbon is removed from the atmosphere, with transport to deeper depths leading to greater storage (Kwon et al., 2009) and lower levels of atmospheric partial pressure of CO_2.

Sinking particles provide the base of the food web for many organisms resident in the mesopelagic zone, such as microbes and non-migrating zooplankton (Jackson, 1993). Consumption by microbes typically leads to a reduction of the sinking particle flux through dissolution and respiration of the organic carbon within the particles. Larger organisms, such as zooplankton, can cause a reduction in particle flux via fragmentation, consumption and respiration of the particles, but may also enhance sinking particle flux via the production of faster sinking faecal pellets (Steinberg and Landry, 2017; Turner, 2015). In addition, abiotic processes, such as disaggregation of fragile particles or aggregation of colliding particles, change particle fluxes (Burd and Jackson, 2009).

Regardless of the exact mechanism, the mass balance of particle flux has to be conserved at steady state. In other words, the attenuation (loss) of carbon flux over a defined depth interval, plus the carbon transported to this depth interval via e.g. physical transport (Boyd et al., 2019), should equal the accumulation of carbon within that depth interval in the form of non-sinking carbon (e.g. via respiration as CO_2, solubilisation/dissolution, incorporation into biomass or transformation to other forms of non-sinking matter). Such mass balance appears, however, elusive with many studies failing to reconcile carbon flux attenuation with biological activity (Baltar et al., 2009; Boyd et al., 1999; Burd et al., 2010; Reinthaler et al., 2006; Steinberg et al., 2008; Uchimiya et al., 2018). The first balanced carbon budget for the mesopelagic zone was observed in the temperate North Atlantic (Giering et al., 2014). Intriguingly, the budget at this site could only be balanced when the entire mesopelagic zone was considered: the depth-resolved budget showed an excess supply of carbon (i.e. more flux attenuation than non-sinking carbon accumulation) in the upper mesopelagic zone, and a deficit in the lower mesopelagic zone (Giering et al., 2014). There was no clear reason for this imbalance, and suggested explanations included vertical changes in the ecosystem with depth or an undetermined vertical transfer.

One of the key assumptions of the North Atlantic carbon budget was that the system was at steady state (Giering et al., 2014). For large parts of the ocean, this assumption is problematic due to strong seasonal cycles in export fluxes (Henson et al., 2015), which can lead to misestimates of carbon supply via sinking particles of up to 25% (Giering et al., 2017). In addition, in non-steady state conditions, carbon reservoirs in the interior ocean, such as non-sinking organic matter accumulated at depth from previous export or subduction events (Boyd et al., 2019; Dall'Olmo and Mork, 2014), may serve as a food source for the organisms living there (e.g. Calleja et al., 2019) and hence need to be considered in carbon budgets.

Here, we address the scale of this accumulation and subsequent consumption of non-sinking particulate matter in the mesopelagic zone in order to test the hypothesis that it serves as an important food source for the mesopelagic biota and so needs to be considered for carbon budgets. We further investigated whether depth-resolved budgets under non-steady state conditions show the previously observed mismatch of excess supply of carbon relative to consumption in the upper mesopelagic zone (and vice versa in the lower mesopelagic zone). To do so, we collected high-resolution vertical profiles of particulate organic carbon concentrations and fluxes in the mesopelagic zone during a Southern Ocean spring bloom near South Georgia.

2. Material and Methods

2.1. Study site and sampling strategy

Particle profiles were collected as part of the COMICS Programme (Controls over Ocean Mesopelagic Interior Carbon Storage) (Sanders et al., 2016) on the RRS Discovery. The first cruise (DY086) targeted the phytoplankton spring bloom downstream of South Georgia in the northern Scotia Sea in Nov/Dec 2017. The study site was chosen to be near the long-term observation station 'P3' (52.4 °S, 40.1°W; Manno et al., 2015) (Fig. 1). Because of the island-derived iron supply, the region is a hot spot of biological productivity and particulate carbon flux compared to the surrounding high nutrient, but low chlorophyll (HNLC) Southern Ocean (Atkinson et al., 2001; Borrione and Schlitzer, 2013). The cruise was deliberately centred in an area of low current speed, weak mesoscale variability, and retentive circulation between the Polar Front (to the West and North) and the Southern Antarctic Circumpolar Current Front (to the South) (Matano et al., 2020; Meredith et al., 2003; Venables et al., 2012). We visited P3 three times for ~7 days each: 15 Nov – 22 Nov (P3A), 29 Nov – 5 Dec (P3B), and 9 Dec – 15 Dec 2017 (P3C).

2.2. Standard water sampling and stand-alone pumping system (SAPS)

Concentrations of particulate organic carbon (POC) were measured from 12 CTD profiles and five Stand-Alone Pump Systems (SAPS; Challenger Oceanic) profiles. Water samples for POC concentrations were collected from 12 depths (approximately 5, 20, 40, 50, 75, 100, 150, 250, 350, 500, 750 and 1000 m depth) using Niskin bottles fitted onto a stainless steel CTD rosette. 1000 or 2000 mL were filtered onto pre-combusted (400°C, 12 h) GF/F filters (0.7-μm nominal pore size, 25 mm; Whatman), briefly rinsed with MilliQ water to remove salts, dried (50°C, overnight) and analysed on shore. On shore, the filters were fumed with HCl (35%, 24 h), dried (50°C, >24 h), and pelleted in tin discs (Elemental microanalysis). The samples were analysed for POC using a Thermo Fisher Scientific FLASH 2000 Organic Elemental Analyser. POC calibration was performed at the beginning of each batch using a series of caffeine standards of varying weights (1–5 mg) with known percentage content of carbon. Reference standards were included in each batch after every 10 samples to check the instrument precision (<1%, n = 72, 1 SD) and drift. If needed, a drift correction was applied. All samples were corrected for filter blanks. As the adsorption of dissolved organic carbon was not measured, 10.9 μg of carbon was subtracted from each POC bottle measurement (based on mean absorption found by Cetinić et al. (2012).

We further determined POC concentrations of two size classes (<53 μm and >53 μm) using in situ large-volume filtration. SAPS were deployed at five depths between 5 and 500 m depth and filtered, on average, 412 L (between 66 and 738 L depending on deployment depth). A full description of the methods and data interpretation is published by Preece et al. (in prep.).

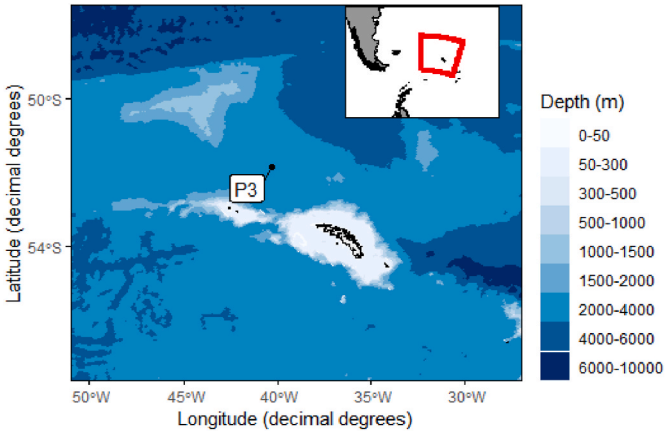

Fig. 1. Long-term observation station 'P3' (52.4 °S, 40.1°W) in the vicinity of South Georgia. Plotted using *ggOceanMaps* (Mikko, 2022).

2.3. Marine Snow Catchers (MSC)

Profiles of suspended, slow-sinking and fast-sinking particles were collected using the Marine Snow Catcher (MSC) (Giering et al., 2016; Riley et al., 2012). During each visit, three particle profiles were collected with 4–5 depths chosen based on the mixed layer depth (MLD). Typically, these depths were: MLD +10 m, MLD +50 m, MLD +100 m, 250 m and 500 m. Opportunistically, other depths (in the upper 250 m or at 1000 m) were also sampled. All MSCs for an individual profile were deployed within 2 h of each other, though variability between profiles collected during each visit was low. Profiles were collected during daylight hours except for two occasions (deployments to 60 m and 150 m on 18th Dec 2017). A full description of how the MSC is deployed and sampled is described by Giering et al. (2016) with slight modifications. Most notably, a tray (polypropylene, 18.5 cm diameter, 4 cm height with a total volume of ~1 L) was secured to the bottom of the base section to collect the fast-sinking fraction.

Briefly, after a 2-h settling period, suspended particles were collected from the middle tap (4–5 L; 'top'). To drain the top section, the middle tap was opened fully and the bottom tap opened by approximately 30° to reduce resuspension of slow-sinking material. Draining typically took 30 min. Slow-sinking particles were collected by carefully syphoning the water from above the tray (4–5 L; 'base'). The tray, containing the fast-sinking particles (1 L; 'tray') was then sealed with a lid, removed, and stored at 2–4 °C until further analysis. We did not observe any large aggregates ('marine snow'; >0.5 mm diameter) until the end of the cruise; however, the fast-sinking fraction was visibly enriched in organic matter. Each fraction was filtered and analysed for POC as for standard water samples (Section 2.2). Typical filter volumes were 1000 mL for suspended and slow-sinking particles, and 150–350 mL for fast-sinking particles.

Concentrations of suspended, slow-sinking and fast-sinking particles (p_{sus}, p_{slow}, and p_{fast}, respectively) were calculated as follows.

$$p_{sus} = p_{top}$$

$$p_{slow} = (p_{base} - p_{top}) \times V_{base} / V_{MSC}$$

$$p_{fast} = (p_{tray} - p_{base}) \times V_{tray} / (A_{tray} \times h_{MSC})$$

where p is the particle concentration (μg L^{-1}) in the top, base or tray sample, V_{base} is the volume of the base section (8 L), V_{MSC} is the volume of the MSC (95 L including base), V_{tray} is the volume of the tray (~1 L, measured for each deployment), A_{tray} is the area of the tray (0.026 m^2) and h_{MSC} is the height of the MSC (1.58 m).

Fluxes of slow-sinking and fast-sinking particles (F_{slow} and F_{fast}, respectively) were calculated as

$$F_{slow} = p_{slow} \times V_{MSC} / (A_{MSC} \times t)$$

$$F_{fast} = p_{fast} \times v_{fast}$$

where A_{MSC} is the area of the MSC base (0.06 m^2), t is the settling time (2 h), and v_{fast} is the average sinking velocity of the fast-sinking fraction, for which we here assumed a range of sinking velocities. As upper bound for the flux estimates, we applied a sinking velocity of 60 m d^{-1} based on particle-specific in situ sinking velocity measurements at 500 m depth (66 ± 47 m d^{-1}; particle diameter of 0.5–2.3 mm; Iversen, pers. comm.) and Polonium-derived sinking velocities, which indicate bulk velocities (i.e. weighted average velocity of slow- and fast-sinking particles) of 44–58 m d^{-1} at 60 m depth and increasing up to 163–182 m d^{-1} at 350 m depth (Villa-Alfageme et al. 2022). An absolute lower flux estimate (i.e. $F_{slow} + F_{fast}$) was calculated by assuming that the observed concentration gradient in the MSC developed within exactly 2 h (equivalent to a sinking velocity v_{fast} of 18 m d^{-1}), which is an underestimate because (1) a substantial fraction of particles likely arrived in the base section much sooner, (2) any turbulences created during sampling would have reduced the apparent concentration gradient between top and base section and hence flux estimates.

2.4. PELAGRA sediment traps

Flux profiles between ~90 and 500 m were further measured using neutrally buoyant sediment traps (PELAGRA) (Lampitt et al., 2008). PELAGRA sampling cups were filled with 10% formaldehyde hypersaline solution and collected material for ~24 h. On shore, samples were split into quarter subsamples (Folsom splitter; Aquatic Research Instruments) and zooplankton swimmers removed. One quarter subsample was further split to obtain a final subsample (either 1/16th or 1/64th) for POC analysis following the methods described above (Section 2.2) with slight modifications. Subsamples were filtered onto pre-combusted (500°C overnight) and pre-weighed GF/F filters (0.7-μm nominal pore size, 25 mm diameter; Whatman), rinsed with buffered MilliQ water (0.025 g L^{-1} of disodium tetraborate, anhydrous; Fisher Scientific), and dried (40°C, overnight) for on-shore analysis. On shore, POC samples were fumed (35% HCl, overnight), dried (50°C, overnight), and pelleted using tin discs (30 mm; Elemental Microanalysis). Blanks of the trap preservative were created by filtering 30 mL of preservative onto a GF/F and handling in the same way as the samples. POC was analysed at the Stable Isotope Facility, University of Southampton, on an Elementar Vario Isotope Select. The limit of detection for the instrument was 4.88 μg of C and the analytical precision was <1%. The tin capsules had a mean blank value below the detection limit of the instrument. Filter blanks (pre-combusted, rinsed with borate-buffered MilliQ) had a mean blank value of 17.3 ± 2.4 μg of C. Acetanilide standards were run at the beginning and end of each run and algae (bladderwrack, 1.25 ± 0.02% N and 33.67 ± 0.29% C; Elemental Microanalysis) standards followed by a blank were run every five samples to track instrument performance.

POC fluxes (F in mg C m^{-2} d^{-1}) were calculated by normalising to the collection area of the PELAGRAs (0.115 m^2) following equation, $F = m\ (t\ A)^{-1}$, where m is the carbon mass (in mg), t is the collection time (in days), and A is the surface area of the opening of the collection funnel (in m^2).

2.5. Glider-derived POC concentrations and fluxes

Three gliders surveyed the study region between Oct 2017 and Feb 2018 as part of the GOCART project (Gauging ocean Organic Carbon fluxes using Autonomous Robotic Technologies). A full description of the glider mission, capabilities and data are published by Henson et al. (2022). For this study, we are focussing solely on the time period of the cruise and on data from the optical backscattering sensor (at 700 nm). Henson et al. (2022) provide a comprehensive description of the method on how POC fluxes were derived from the glider data. Briefly, we used a running minimum-maximum filter to isolate spikes (i.e. 'large particles') from a baseline signal (i.e. 'small particles') following Briggs et al. (2011). Spikes below a minimum threshold based on deep ocean 'blanks' were set to zero, eliminating some instrument noise and discretization effects. This value was equivalent to particles with a diameter of approximately 420 μm (following the approximate scaling between spike height and size; Briggs et al., 2013), so the 'large particle' signal is interpreted as representing particles >420 μm. 'Small particles' and 'large particles' were each binned into 10-m depth and 12-h time bins. POC concentrations were calculated using a linear regression between backscatter and CTD bottle data (15 calibration casts resulting in a final n = 141; for POC analysis methods see Section 2.2; for the regression details see Henson et al., 2022). Glider-derived POC concentrations and POC concentrations measured from physical samples agreed well (Supplementary Fig. S1). Bulk sinking velocities of the 'large particles' were estimated using the plume-tracking method (Briggs et al., 2011, 2020) with a modification to allow an increase in sinking velocities with increasing depth (Villa-Alfageme et al., 2022). Resulting bulk 'large-particle' sinking velocities ranged from ~40 m d^{-1} in the surface to ~130 m d^{-1} at 1000 m. The sinking velocity of 'small particles' was

assumed to be 2.5 m d^{-1} (sinking rate for large diatoms; Bannon and Campbell (2017). POC flux was then calculated by multiplying POC concentrations with sinking velocities and summing 'small particle' and 'large particle' fluxes. Lower and upper estimates were calculated by varying the sinking velocities: For the lower estimate, sinking velocities for 'small particles' and 'large particles' were set to 0 m d^{-1} and 50% of the 'best estimate', respectively. For the upper estimate, 'small particles' and 'large particles' were set to 10 m d^{-1} (Briggs et al., 2020) and 100% of the 'best estimate', respectively. The estimates of the deepest glider bin (990–1000 m; nominally 995 m) has the highest uncertainties because the glider turned at this depth and the motion of the particles through the backscattering sensor was hence less reliable. We therefore used the next deepest bin (980–990 m; nominal 985 m) as representative deep flux.

2.6. Calculation of vertical and temporal changes

We used the glider-derived high-resolution POC concentration and flux data to investigate spatiotemporal changes. Specifically, we aimed to calculate the change in POC concentration at any specific depth range and to estimate the POC fraction that can be accounted for by the input of material to the depth range of interest. To quantify the change in POC concentration within each depth bin over time ('temporal changes'), we calculated the difference from one 12-h bin to the next, and then calculated the average change in POC concentration for each visit. This value is the average rate of change in POC concentration during each visit (~7 days) and is expressed in absolute terms (mg C m^{-3} d^{-1}) or as percentage daily change (d^{-1}) of the average POC concentration (in mg C m^{-3}) during that period. We calculated the absolute difference in POC concentration within each depth bin relative to the average concentration of that depth bin (in mg C m^{-3}) throughout the study period (15 Nov 2017–15 Dec 2017). Finally, we calculated the vertical difference in POC concentrations (in mg C m^{-3}) for each POC profile by subtracting the concentration at a given depth bin from the highest POC concentration of that profile.

For fluxes, we quantified the 'vertical changes' for each profile by subtracting the deeper depth bin, which was expected to have a lower flux following flux attenuation, from the depth bin immediately above (e.g. flux [bin 30–40 m] - flux [bin 40–50 m]) and dividing by the bin size (i.e. 10 m; resulting in unit mg C m^{-3} d^{-1}). We then calculated the average of each depth bin for each visit and computed the running mean (n = 5) to reduce the noise. The resulting values showed the average vertical change during each visit (~7 days) and can be expressed in absolute terms (mg C m^{-3} d^{-1}) or percentage daily change (d^{-1}) of the average POC concentration (in mg C m^{-3}) during that period.

2.7. Export depth based on productive layer

The depth of export, and hence the boundary between epipelagic and mesopelagic zone, was here chosen to be the productive layer depth. The productive layer is the layer in which particles can be produced photosynthetically and is typically either the euphotic zone depth or the mixed layer depth, whichever is deeper (Dall'Olmo and Mork, 2014). Following the recommendations by Buesseler et al. (2020), we estimated the productive layer depth from the glider time-series (Henson et al., 2022) using a modification of the metric by Owens et al. (2015). For each glider profile, the productive layer depth was defined as the deepest point at which chlorophyll was higher than 10% of the maximum chlorophyll concentration for that profile. During the cruise period, the estimated productive layer depths were always deeper than the euphotic zone (0.1% PAR) and exceeded the seasonal mixed layer depth (0.05 kg m^{-3} density difference from surface values) by a median value of 13 m.

The estimated export depths were 92.5 m ± 8.1 m, 91.5 m ± 12.9 m and 88.5 m ± 10.4 m for the first, second and third visit, respectively. As the glider-derived high-resolution POC concentrations and fluxes were binned in 10-m bins, we used the bin 90-100 (nominal '95 m') as export depth throughout the manuscript.

3. Results

3.1. POC concentrations

The glider backscatter-derived POC concentrations generally matched observations between the mixed layer and 500 m depth (Figs. 2 and 3). The gliders may have underestimated POC concentrations in the mixed layer and below 500 m compared to CTD bottle data. In the mid-water column, the CTD-derived POC concentrations appeared slightly higher and SAPS-derived a bit lower. Overall the high-resolution backscatter-derived POC profiles appear to describe the observed vertical profiles well. Hereafter, POC concentrations will refer to the high-resolution glider backscatter-derived values unless otherwise stated.

POC concentrations showed the typical vertical gradient with higher concentrations in the surface ocean (142–252 mg C m^{-3} at 0–10 m) and a rapid decline in the upper mesopelagic zone to 24–40 mg C m^{-3} at 190–200 m depth. Below this depth, POC concentrations declined slowly to 7–9 mg C m^{-3} at ~1000 m depth (Fig. 3). Over the course of the cruise, POC concentrations in the surface (0–10 m) declined from 252 to 181 to 142 mg C m^{-3} during the first, second and third visit to P3, respectively. This decline concurred with a decrease in the phytoplankton community in terms of chlorophyll concentrations in the mixed layer (from 3.8 ± 1.9 mg Chl m^{-3} during the first visit to 1.3 ± 0.3 mg Chl m^{-3} during the third visit) (Ainsworth et al., 2023). Throughout the cruise, the phytoplankton community was dominated by large cells (>10 μm), composed predominantly of diatoms such as *Eucampia antarctica* and *Fragilariopsis kerguelensis*, which made up ~95%, ~91% and ~83% of the total chlorophyll in the mixed layer during the first, second and third visit, respectively (Ainsworth et al., 2023).

Conversely, POC concentrations in the upper mesopelagic zone increased during this time, from 24 to 39–40 mg C m^{-3} (at 190–200 m depth). These opposing trends along each depth horizon are clearly illustrated by the temporal anomalies with a change exceeding −120 mg C m^{-3} in the surface ocean (Fig. 4a). As a result of the opposing trends, the initially strong vertical concentration gradient, with a decrease of up to 268 mg C m^{-3} from the surface to 1000 m depth during P3A, became much weaker (Fig. 4b). Towards the end of the third visit (P3C), the concentration gradient from surface to 1000 m depth had decreased to 130 mg C m^{-3}. An average of only 4% of the estimated glider-derived POC concentration (over the entire cruise period and between 95 and 1000 m depth) was associated with 'large particles' (>420 μm in diameter), which agreed well with the scarcity of visible aggregates (>500 μm diameter) in the MSCs.

The high-resolution data further allowed us to calculate rates of change during each visit (i.e. the average rate of change during ~7 days). In the mixed layer, changes were erratic with no clear trend. Throughout the mesopelagic zone, POC concentrations increased during the first and second visit (P3A and P3B; Fig. 5a). During P3B, the average daily increase during the visit was up to 1.2 mg C m^{-3} d^{-1} at 150–170 m depth, equivalent to a daily increase of 2.6% d^{-1} of the POC standing stock (Fig. 5b). This accumulation reversed during our third visit (P3C) when POC concentrations decreased at an average rate of up to −0.8 mg C m^{-3} d^{-1} at 250–270 m depth, equivalent to −2.7% d^{-1} of the POC standing stock at this depth (Fig. 5b).

3.2. POC fluxes

The time-series revealed an overall good match of the glider-derived POC flux estimates and the direct measurements (Fig. 6; Henson et al., 2022). All platforms seemed to agree well around 500 m depth, though near the surface there were some distinct differences. The PELAGRA traps estimated fluxes toward the lower end of the glider-derived

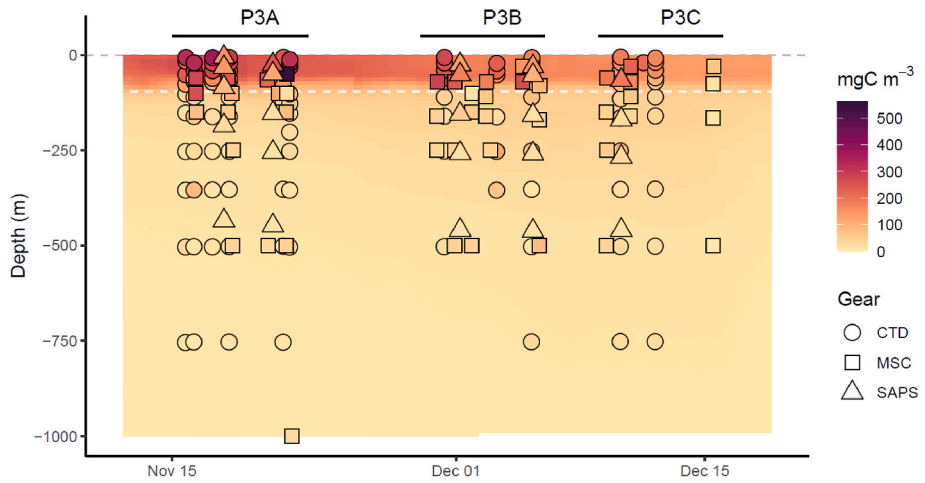

Fig. 2. POC concentrations in the mesopelagic zone during the cruise (range: 0–550 mg C m^{-3}) based on samples collected using Niskin bottles ('CTD' as circles), Marine Snow Catchers ('MSC' as squares) and Stand-Alone Pumping Systems ('SAPS' as triangles). Background shows POC concentrations based on glider backscatter intensity. Sampling periods during visits P3A, P3B and P3C are indicated by the horizontal bars. White dashed line indicates the mixed layer depth.

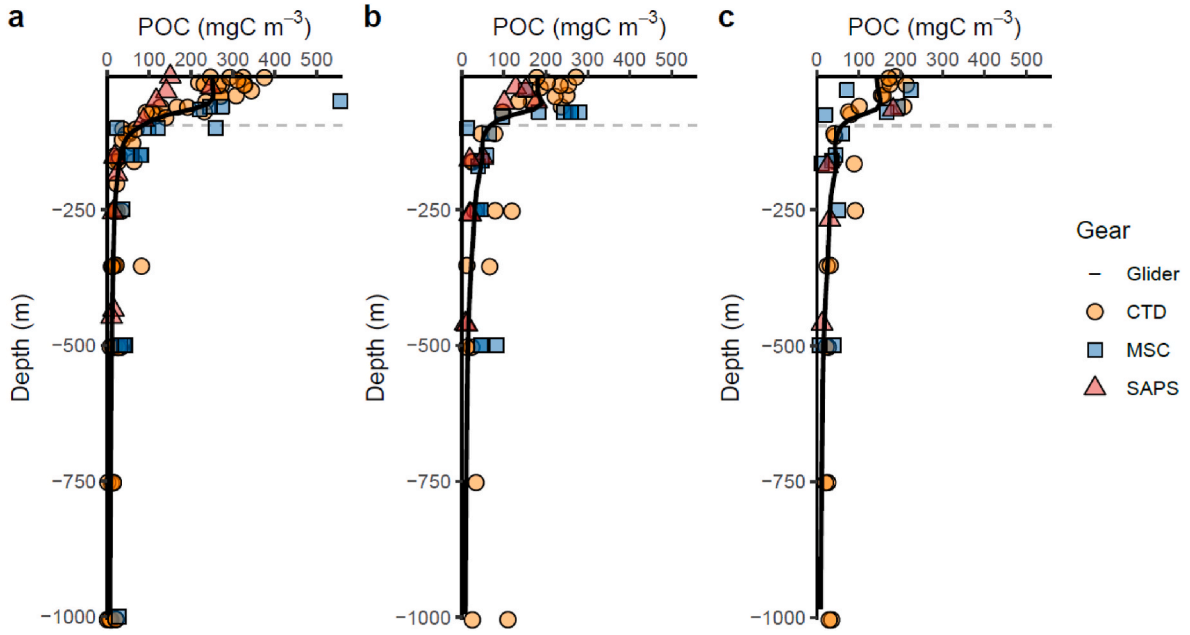

Fig. 3. Vertical profiles of POC concentrations during the three station occupations. (a) P3A: Nov – 22 Nov, (b) P3B: 29 Nov – 5 Dec, and (c) P3C: 9 Dec – 15 Dec 2017. Symbols identify data source: CTD bottle data (open circle), glider-derived (solid line), Marine Snow Catchers (MSC) time-zero samples (open square), and Stand-Alone Pumping Systems (SAPS, open triangle). Grey dashed line indicates the mixed layer depth.

uncertainty envelope, with largest discrepancies near the mixed layer depth during P3A and P3C. This observation is in line with previous observations that sediment traps tend to underestimate flux in the upper ocean owing to a range of factors, such as hydrodynamic disturbances and dissolution (Buesseler et al., 2007). Furthermore, the conical shape of the PELAGRA trap might have led to undersampling of small particles throughout the water column (Baker et al., 2020). A comparison of the two size classes of POC determined by the SAPS revealed a significant increase in larger particles (>53 μm) with depth from 20% of total POC in the upper 100 m (range: 7–37%) to 41% of total POC between 400 and 500 m depth (range: 31–53%; $p = 0.03$, $R^2 = 0.15$, $n = 24$). MSC-derived flux estimates, on the other hand, were towards the upper end of the glider-derived uncertainty envelope. Noteworthy here is the uncertainty range for the MSC: the open squares indicate the minimum "true fluxes" based on the concentration gradient observed after 2 h of settling (Fig. 7), whereas the blue squares consider fast-sinking particles that had likely arrived in the bottom section in shorter than 2 h. The MSC uncertainty envelope generally straddled the glider-derived best estimate, suggesting overall good agreement between the two estimates. Hence, hereafter, POC fluxes will refer to the high-resolution backscatter-derived values unless otherwise stated.

POC fluxes followed the typical pattern of high fluxes in the surface ocean (755–1435 mg C m^{-2} d^{-1} at 50–60 m depth) that were attenuated rapidly in the upper mesopelagic zone (from 287 to 646 mg C m^{-2} d^{-1} at 90–100 m to 141–215 mg C m^{-2} d^{-1} at 190–200 m depth) and more slowly in the lower mesopelagic zone (down to 56–74 mg C m^{-2} d^{-1} at 980–990 m depth) (Fig. 7). Throughout the cruise, POC export (defined as flux at 95 m) declined from 646 to 409 to 287 mg C m^{-2} d^{-1} during the first, second and third visit, respectively (Table 1). This change in flux broadly mirrored the decline in primary production (1948 ± 89, 1488 ± 146 and 1221 ± 56 mg C m^{-2} d^{-1} during the first, second and third visit, respectively; Henson et al., 2022) estimated from incubation

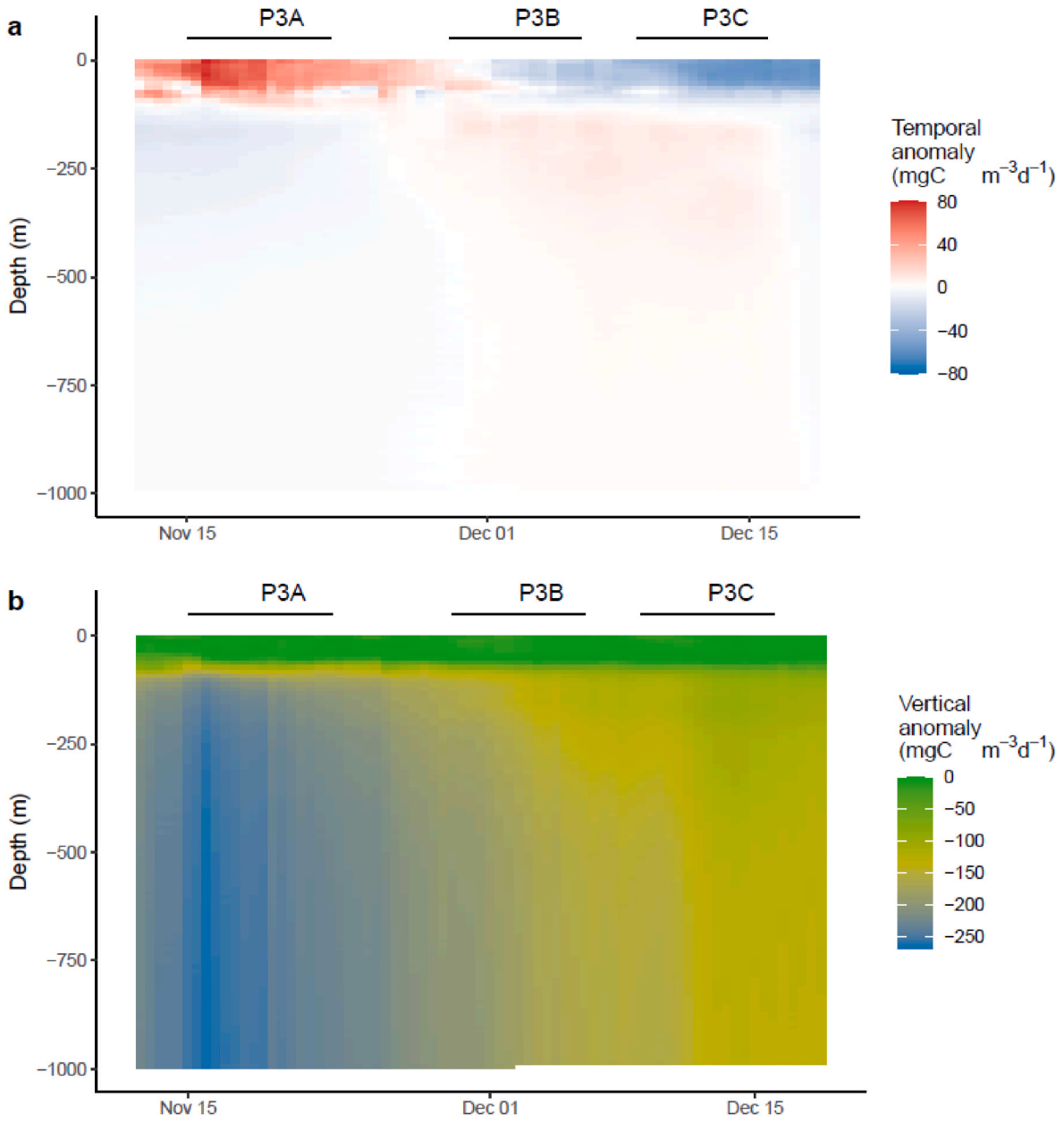

Fig. 4. Change in POC concentrations. (a) Change over time at a given depth normalized to the average concentration at that depth (in 10-m bins). Red indicates a period of higher POC concentration relative to the average at this depth; blue indicates a period of lower POC concentration. (b) Change of POC concentration with depth relative to the surface concentration. Green shades indicate similar concentrations as those at the surface, yellow shades indicate a difference of ~150 mg C m^{-3}, blue shades indicate a difference of ~250 mg C m^{-3} relative to the surface.

experiments and glider-derived light fields based on methods by Mignot et al. (2018). Export efficiencies (export flux as a fraction of net primary production) appeared to decrease over time (33, 27 and 24%, respectively).

Flux attenuation in the upper mesopelagic zone was highest during the first visit with changes of up to 19 mg C m^{-3} d^{-1} (equivalent to 0.22 d^{-1} of the POC concentration) just below the export depth (Fig. 8). The magnitude of this attenuation decreased during the cruise, down to 11 mg C m^{-3} d^{-1} (equivalent to 0.15 d^{-1} of the POC concentration) just below the export depth during the third visit (Fig. 8). The vertical pattern of flux attenuation was not consistent, with higher attenuation rates being maintained much deeper (to ~165 m depth, as defined at the first occurrence when flux attenuation was <2 mg C m^{-3} d^{-1}) during the first visit compared to the second and third visit (to 125 m and 115 m depth, respectively) (Fig. 8a). As a result, transfer efficiency throughout the upper 100 m of the mesopelagic zone (from 95 to 195 m depth) increased during the cruise from 22% to 53–64% during the first, second and third visit, respectively. Transfer efficiency through the remainder of the mesopelagic zone (i.e. from 195 to 985 m depth) decreased throughout the cruise, from 52% during the first visit to 34% and 30% during the second and third visit, respectively (Table 1).

3.3. POC budgets

We compared the attenuation in flux (i.e. how much of the flux was 'lost' to, e.g., respiration, fragmentation, etc.) with the change in stock (i.e. whether the POC concentrations increased or decreased). Integrated over the entire mesopelagic zone and in the upper mesopelagic zone (95–195 m), POC flux attenuation was higher than the observed accumulation of suspended POC during all three visits (Fig. 9a). Between 95

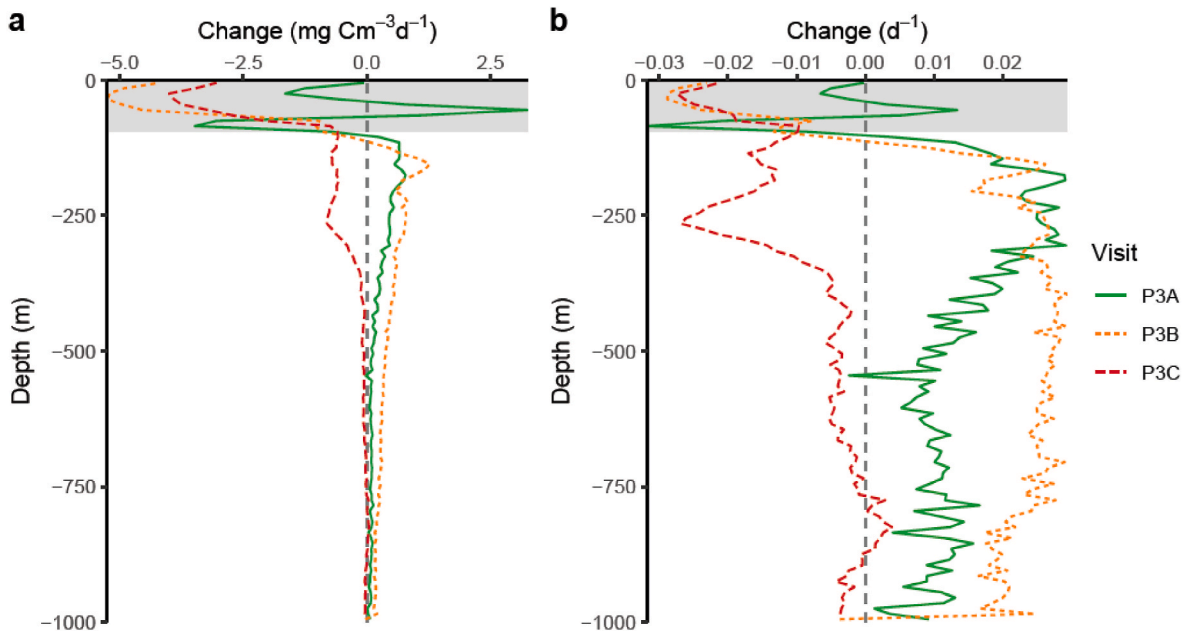

Fig. 5. Change in POC concentration at depth over the duration of the visit expressed as (a) absolute mass (mg C m^{-3} d^{-1}), and (b) fraction of the average POC concentration during that period at that depth (d^{-1}). I.e. the value at 250 m refers to the change of POC concentration at this depth over a 24-h period. Visits P3A, P3B and P3C are shown in solid green, dotted orange and dashed red, respectively. The mixed layer is shaded in grey.

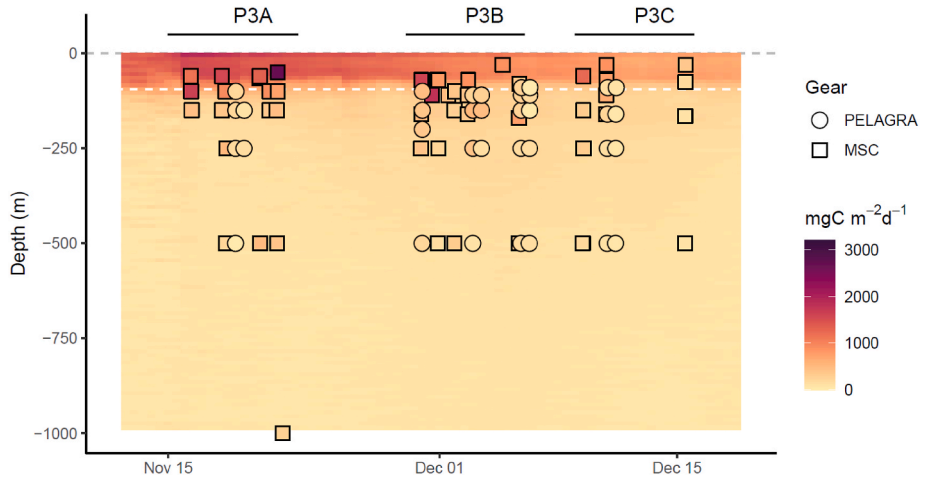

Fig. 6. Time series of vertical flux profiles during the cruise (13th Nov - 18th Dec 2017). Background shading shows fluxes derived based on the glider backscatter. Overlaid are fluxes determined by the Marine Snow Catchers (MSC, squares) and PELAGRA sediment traps (circles). White dashed line indicates the mixed layer depth.

and 1000 m, during the first, second and third visit, respectively, flux attenuation (581, 388 and 302 mg C m^{-2} d^{-1}) exceeded the accumulation of POC in this depth interval (197, 366 and −172 mg C m^{-2} d^{-1}; equivalent to 34, 94 and −57% of the flux attenuation), leaving an excess of 384, 22 and 474 mg C m^{-2} d^{-1} for respiration (and dissolution). Excess was even more pronounced in the upper mesopelagic zone (95–195 m), where flux attenuation (520, 253 and 170 mg C m^{-2} d^{-1}) exceeded POC accumulation (63, 67 and −63 mg C m^{-2} d^{-1}; equivalent to 12, 27 and −37% of the flux attenuation) and allowed 457, 186 and 233 mg C m^{-2} d^{-1} for other consumptive processes. However, in the lower mesopelagic zone, POC flux attenuation during the first and second visit did not supply sufficient carbon to even explain the increase in suspended POC (Fig. 9c): Flux attenuation supplied 61 (uncertainty envelope: 10–186) and 135 (30–361) mg C m^{-2} d^{-1} during the first and second visit, respectively, whereas POC accumulation appeared to be 134 (122–147) and 299 (270–327) mg C m^{-2} d^{-1}. Hence, there seemed to be a deficit of 74 and 164 mg C m^{-2} d^{-1}, though it is noteworthy that the estimates match within the uncertainties. During the third visit, POC stocks appeared to decrease (−109 mg C m^{-2} d^{-1}), hence allowing a total of 241 mg C m^{-2} d^{-1} for consumptive processes over this depth horizon. The budgets are robust in respect of the exact separation depth between upper and lower mesopelagic zone (Supplementary Fig. S2).

4. Discussion

We compared high-resolution estimates of gravitational POC flux and accumulation of POC within the mesopelagic zone over the course of the spring bloom. First, we explore the temporal changes in the POC inventory of the mesopelagic zone under non-steady state conditions and discuss the implications for ocean carbon storage via the biological carbon pump. We then focus on the vertical distribution of these changes by compiling simple carbon budgets. We did not include respiration in

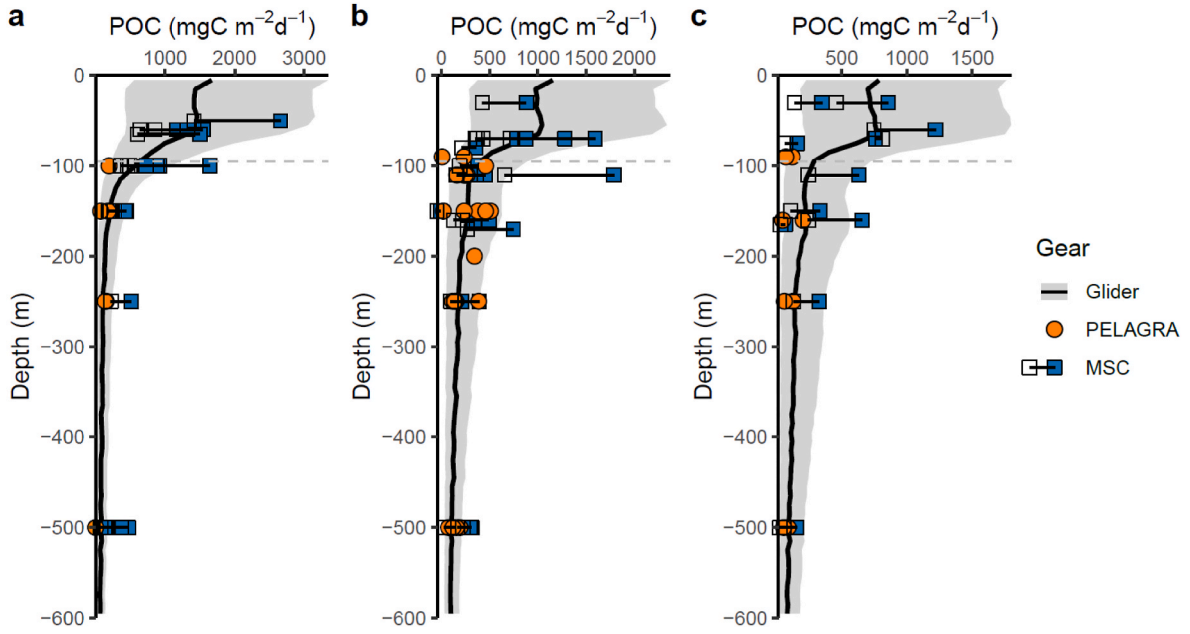

Fig. 7. Vertical flux profiles during the three visits at (a) P3A, (b) P3B and (c) P3C. Black line shows glider-based estimates with lower and upper limits indicated by the grey envelope. Overlaid are fluxes determined by the Marine Snow Catchers (MSC, squares) and PELAGRA sediment traps (orange circles). The absolute lower flux estimate based on the MSCs is indicated by the open squares, whereas the blue squares show their best estimate.

Table 1
Overview of the visits. Primary production (PP) based on incubation experiments and glider-derived chlorophyll and lightfields. Fluxes are based on glider-derived estimates. Export efficiency (ExEff) is the ratio of export flux over PP. The shallow transfer efficiency, T_{100}, is the fraction of export flux that makes it to 100 m below export depth (i.e. 195 m). The lower mesopelagic zone transfer efficiency, $T_{lowerMZ}$, is the fraction of sinking material that reaches 1000 m depth relative to flux at 195 m.

Visit	PP (0–60 m)	'Export': Flux at 95 m	Flux at 195 m	Flux at 985 m	ExEff	T_{100}	$T_{lowerMZ}$
	mg C m^{-2} d^{-1}	mg C m^{-2} d^{-1}	mg C m^{-2} d^{-1}	mg C m^{-2} d^{-1}			
P3A	1948	646	141	74	0.33	0.22	0.52
P3B	1488	409	215	73	0.27	0.53	0.34
P3C	1221	287	185	56	0.24	0.64	0.30

our budgets as the estimation of mesopelagic respiration introduces large uncertainties (e.g. Giering et al., 2014; Giering and Evans, 2022). While, at face value, the budgets balance when considering the entire mesopelagic zone with excess carbon for respiration, a vertical transfer of carbon from the upper to the lower mesopelagic zone appears to be needed, particularly when we factor in that respiration by prokaryotes and zooplankton occurred (Evans et al., this issue). We discuss the potential transport mechanisms that could help resolve this vertical imbalance.

4.1. *Effect of the spring bloom on the mesopelagic environment*

The mesopelagic zone is typically considered an oligotrophic environment owing to its relatively low resource availability, with POC concentrations typically similar to those observed in surface water of oligotrophic regions (25 mg C m^{-3}; Supplementary Fig. 3) (Martiny et al., 2014), which we also observed during our first visit. Here, however, we observed a strong enrichment in POC concentrations throughout the cruise (up to 46 mg C m^{-3} at 165 m during the third visit), equivalent to levels observed in temperate surface waters (Martiny et al., 2014). This accumulation was likely driven by the high amount of organic matter that was exported from the mixed layer throughout the bloom. Export fluxes during our first visit (646 mg C m^{-2} d^{-1}) were on the high end of observed global export fluxes (Henson et al., 2015; Mouw et al., 2016). Though high, these fluxes were consistent with the high primary production rates measured during our study (~2000 mg C m^{-2} d^{-1} during the first visit; Henson et al., 2022). The resulting export efficiency, i.e. the ratio of export over primary production, of 24–33% was consistent with large-scale satellite-derived estimates for our study region (20–30%, Henson et al., 2012; though see Arteaga et al. (2018) for a comparison of satellite-derived estimates).

In terms of temporal changes, the mesopelagic zone is often considered at steady state with any particulate organic matter entering it meeting one of two fates: (1) it stops sinking through fragmentation or consumption and is converted to dissolved carbon (as either dissolved organic carbon or dissolved inorganic carbon) or (2) it leaves the mesopelagic zone as part of the sinking particle flux. Here, in addition to these processes, we observed that a substantial fraction of the particulate flux (34–94%) appeared to have slowed down or stopped sinking and accumulated as particulate matter in the upper mesopelagic zone. This accumulation is consistent with observations in the Nordic Sea (~70°N 3°E) of a seasonal accumulation of small particles in the mesopelagic zone (Dall'Olmo and Mork, 2014). Moreover, it is consistent with estimates of particle fragmentation rates during high-flux events in the North Atlantic and Indian sectors of the Southern Ocean (30–60%; Briggs et al., 2020).

The gliders observed a concomitant increase in fluorescence down to 400 m depth (Henson et al., 2022), suggesting that the accumulated POC was associated, at least in part, with relatively fresh phytoplankton. Measurements of fast repetition rate fluorescence (Kolber et al., 1998) on the material collected by the sediment traps at 500 m during the second visit (2nd Dec) suggested that it contained phytoplankton cells with photosynthetic efficiencies (0.33 ± 0.02 F_v/F_m) similar to those found near the surface (0.3–0.4 F_v/F_m; Moore et al., unpublished). On-board incubations of surface phytoplankton communities in complete darkness showed that even after 16 days (end of incubation) the phytoplankton cells continued to be photosynthetically viable without a marked decrease in their physiological status (from ~0.36 F_v/F_m to ~

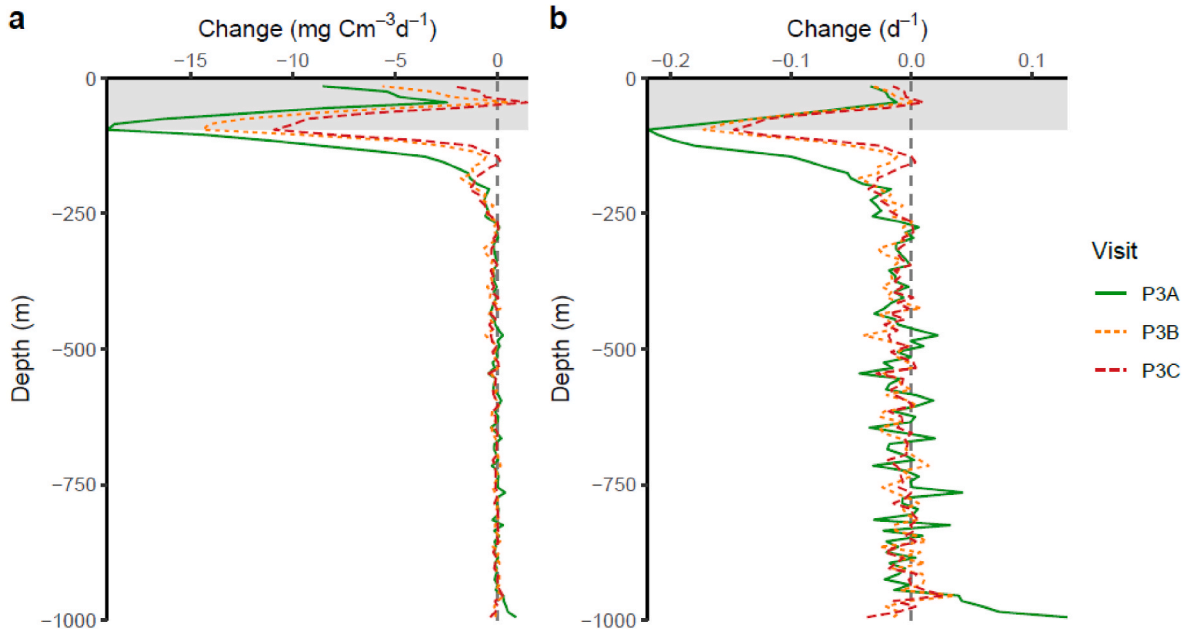

Fig. 8. Change in vertical POC flux with depth during each visit expressed as (a) absolute mass (mg C m^{-3} d^{-1}), and (b) fraction of POC concentration at that depth (d^{-1}). I.e. the value at 250 m refers to the change of POC flux from 249 m depth to the flux at 250 m depth. Visits P3A, P3B and P3C are shown in solid green, dotted orange and dashed red, respectively. The mixed layer is shaded in grey.

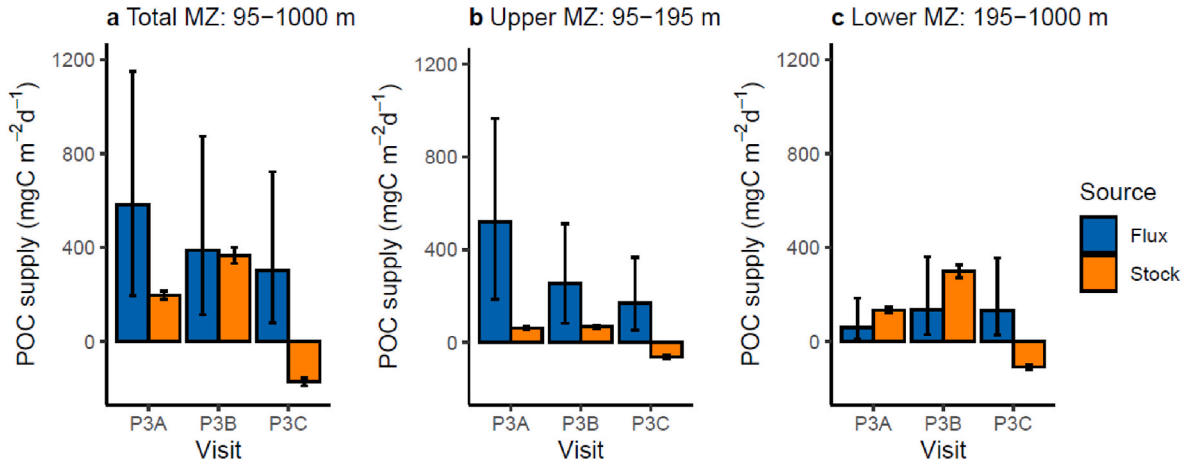

Fig. 9. Mesopelagic carbon budget with different depth horizons. Comparison of organic matter supply via sinking particles (blue) to the accumulation (or loss at P3C) of POC (orange) during the three visits (P3A, P3B and P3C) for (a) the entire mesopelagic zone from 95 to 1000 m depth, (b) the upper mesopelagic zone from 95 to 195 m depth, and (c) the lower mesopelagic zone from 195 to 1000 m depth. Values (mg C m^{-2} d^{-1}) are integrated over the three depth horizons (905, 100 and 805 m, respectively). Error bars show, for fluxes, upper and lower estimates for fluxes based on sinking rate assumptions, and, for stocks, standard deviation of estimated POC concentrations.

0.31 F_v/F_m) (Moore et al., unpublished). In addition, ship-board radiotracer experiments indicated that mesopelagic microbes were likely not remineralizing sinking healthy diatom cells (Ainsworth et al., 2023). Hence, active phytoplankton cells could have spent a considerable time sinking through the mesopelagic zone before undergoing remineralization owing to consumption or cell depth.

Only a relatively small fraction (22%) of the exported material was transferred through the upper mesopelagic zone (95–195 m depth) during the first visit, indicating that particle sinking velocities slowed down. During this period, we did not observe any large aggregates (>0.5 mm diameter) in the MSCs but instead a high abundance of large diatoms and diatom chains (visual inspection and in situ camera systems; Giering et al., 2020). Though we cannot conclusively say why these particles slowed down and eventually stopped sinking, it was probably a combination of vertical changes in seawater density (e.g. MacIntyre et al., 1995), particle buoyancy regulation of viable cells like diatoms (e.g. Moore and Villareal, 1996), dissolution and microbial remineralization (e.g. Benner and Amon, 2015; Hansell and Orellana, 2021), and fragmentation or disaggregation (Briggs et al., 2020). The slow-down in sinking velocities of these particles in the upper mesopelagic zone would lead to a gross accumulation in POC, as observed here. It would further explain why particles became more homogeneous in appearance (such as size, roundness and solidity) towards the lower mesopelagic zone (Giering et al., 2020): the proportion of denser, non-viable particles would become relatively more important for particle flux with depth.

The accumulation of organic matter in the upper mesopelagic zone was, however, transient, as it only occurred during the first two visits, after which we observed a decrease of the accumulated POC (Fig. 5). Overall, mesopelagic POC concentrations appeared to follow the pattern

of surface ocean seasonality, albeit delayed by approximately 2–3 weeks. Glider-derived primary production showed peak production rates during and just after the first visit (P3A; around 17th - 29th Nov) (Henson et al., 2022), whereas POC concentrations in the upper mesopelagic zone peaked around 3rd - 13th Dec (Fig. 4a). One may hence consider two different phases: a net accumulative phase when particle flux attenuation delivered more carbon than was lost due to heterotrophic and dissolution processes, followed by a net consumptive phase when both particle flux and carbon stock were drawn down, i.e., consumed. During the consumptive phase, the 'reservoir' of suspended POC supplied carbon equivalent to 32–82% of the flux supply (Fig. 9). This reservoir is typically not considered for mesopelagic carbon budgets, which are often considered to be at steady-state (e.g. Collins et al., 2015; Giering et al., 2014; Santana-Falcón et al., 2017; Steinberg et al., 2008).

We propose that, as the system was in non-steady state, the whole mesopelagic ecosystem was likely not very active during the first visit (P3A) as indicated by low microbial activity (lowest observed leucine assimilation rates throughout the cruise; Rayne et al., 2022). As a result, any sinking matter in the mesopelagic zone could escape consumption. This effect would not be apparent in the upper mesopelagic zone where particles may have slowed down or stopped sinking from processes other than consumption. It is, however, in line with the observation that transfer efficiency in the lower mesopelagic zone was highest during P3A: 52% of the sinking material was transferred from 195 to 1000 m depth (Table 1).

As the bloom progressed, three things appeared to have happened. (1) The surface ocean changed to a more heterotrophic system as indicated by the decline in primary production and POC concentrations in the surface ocean (Figs. 2 and 4) and the increase in prokaryotic activity (Rayne et al., 2022). This increase in heterotrophic activity may have resulted in more tightly packed, faster sinking particles. Based on in situ imaging data (holographic camera; see Giering et al. (2020)), the proportion of detritus- and faecal-pellet-like particles was highest during the third visit: The contribution of clearly identifiable diatoms decreased from 30% to 13% estimated carbon biomass (average between surface and 255 m depth), while detritus-like particle biomass increased from 65 to 77% (Giering, unpublished data). Note, however, that zooplankton biomass did not appear to have changed over the course of the study. (2) These more compact, likely faster sinking particles appeared to have sunk through the upper 100 m of the mesopelagic zone relatively unperturbed (in terms of quantity) during the second and third visits, with a transfer efficiency T_{100} of 53–64%. (3) By the time of the second visit, the mesopelagic ecosystem appeared to have 'switched on': during P3B and P3C, the transfer through the lower part of the mesopelagic zone ($T_{lowerMZ}$) decreased to ~30–34%. (Note, the rates are on top of the consumption of suspended POC). This increased activity was likely caused by microbial activity: microbial biomass, leucine uptake, leucine respiration and leucine assimilation efficiencies - which can be used as proxy for growth efficiencies - had increased throughout the mesopelagic zone (Rayne et al., 2022).

The resulting effect is peculiar: regardless of the time of the bloom, rates of PP and size of export flux, the flux that reached 1000 m depth was relatively constant throughout the cruise (56–74 mg C m^{-2} d^{-1}). If this phenomenon was widespread, our observation would have direct implications for estimating the strength of the biological carbon pump in the Southern Ocean. In particular, the use of surface conditions (e.g., satellite-derived parameters such as primary production or export efficiency) to estimate ocean carbon storage would likely overestimate the impact of surface blooms for transporting carbon to depth.

4.2. Mesopelagic POC budgets - unresolved vertical transfer

Our POC budgets showed a similar vertical separation in the dynamics of the upper and the lower mesopelagic zone as observed in the North Atlantic (Giering et al., 2014). For the North Atlantic budget, the mesopelagic zone was, as in our case, separated at 100 m below the mixed layer (i.e. upper and lower mesopelagic zone = 50–150 m and 150–1000 m, respectively), making both studies directly comparable. In both cases, the use of a dynamic upper boundary for the mesopelagic zone (see also Buesseler and Boyd, 2009) was critical for correctly assessing the mesopelagic carbon budget (Giering et al., 2014). A similar vertical mismatch between source and sink was also observed in the subarctic and subtropical western North Pacific for 200–500 m vs 500–4810 m during several short (<1 month) field campaigns (Uchimiya et al., 2018). The latter study suggested that the vertical uncoupling can be partially resolved by *"assuming a temporal uncoupling between supply and consumption, which partly equilibrates the carbon budget over a longer (yearly) time scale"* (Uchimiya et al., 2018). A steady-state assumption over a longer time scale (yearly) may also be valid in our study region. However, in our case, we directly accounted for temporal mismatch in POC supply and consumption by tracking mesopelagic POC accumulation, and we still found that measured POC supply by sinking flux was likely insufficient to explain the lower mesopelagic budget in two of the three visits (Fig. 9c). While this mismatch did not quite exceed the uncertainty bounds of our POC flux supply estimates, even our upper bound supply estimates, which only just matched the observed accumulation during visits P3A and P3B, would not have left any room in the lower mesopelagic budget for POC consumption. Hence we find a mismatch in our mesopelagic POC budgets that was logistical rather than temporal.

In addition to temporal decoupling, another suggested cause for the apparent vertical mismatch in previous studies was related to methodological issues concerning the estimates of respiration: Typically, carbon budgets assume that metabolic conversion factors are constant throughout the deep ocean (e.g. Giering et al., 2014). Subtle changes in ecosystem structure, such as decreasing microbial communities and activity, with depth (DeLong et al., 2006; Iversen et al., 2010) could however cause depth variations in the conversion factors and hence introduce apparent over- and underestimates of the true activities. Here, our budgets are based solely on POC flux vs. stock and estimates of respiration are not included. In our case, methodological uncertainties include our flux estimation and any associated parameters that may change with depth. Our POC dataset is in itself consistent as it uses the same method (glider-derived POC) and conversion factors. Backscatter-to-POC conversion factors may differ for suspended and sinking particles and with depth. If aggregates of surface POC material dominate the large-particle signal, this difference is expected to be small (Briggs et al., 2011) and unlikely to introduce mismatches of the order observed here (see also Supplementary Fig. S1). In theory, compact faecal pellets could scatter less light per unit mass than suspended particles (decreasing b_{bp}/POC), but they might also be depleted in organic carbon relative to "fresh" material (increasing b_{bp}/POC). While the conversion of backscatter-to-POC may change with depth and hence may increase uncertainties, bottle POC measurements also suffer from higher inaccuracies at depth owing to the relatively larger effect of contamination of blank signals when concentrations are low. Despite these caveats, our glider-derived estimates of POC concentrations agreed well with direct observations (Figs. 2 and 3). For the exploration of POC concentrations at depth, we believe that the combination of high-resolution optically derived data with more traditional methods such as bottle samples are best.

Methodological uncertainties are higher around the sinking velocity estimates. We applied sinking velocities for large particles that increased with depth and were consistent with independent estimates of sinking velocities (Villa-Alfageme et al., 2022), and we carried out a sensitivity analysis. The resulting fluxes agreed reasonably well with independent flux observations (Figs. 6 and 7). Consequently, methodological issues with sinking POC flux estimates are unlikely to be the primary cause for the observed vertical imbalance. Another source of uncertainty in our budgets is the potential effect of advection on our mesopelagic net accumulation budgets. The study was conducted in an area of low

current speed (Matano et al., 2020), and minimal changes in mesopelagic temperature and salinity were observed over the course of the study (*data not shown*). Therefore, we do not expect advection to explain the substantial discrepancy between lower mesopelagic POC supply and accumulation in two of the three cruise periods.

Hence, the most likely explanation is an unaccounted mechanism that vertically transfers carbon from the upper to the lower mesopelagic zone (as also suggested by Giering et al., 2014). Five mechanisms that can inject particles into the ocean interior have been identified (Boyd et al., 2019) that we have not considered so far, namely the mixed-layer pump, the large-scale physical pump, the eddy-subduction pump, the seasonal-lipid pump and the mesopelagic-migrant pump.

The large-scale physical pump describes the transport of particles by large-scale (>100 km) subduction through Ekman pumping and circulation features and is typically small relative to carbon transport by sinking particles (Boyd et al., 2019). Moreover, though our study site was close to the Southern Antarctic Circumpolar Current Front (Matano et al., 2020), our study site was, according to global models, located in a region of low subduction rates (Liu and Huang, 2012). Particles can also be subducted by eddies, a mechanism called the eddy-subduction pump (Boyd et al., 2019). The study site, located in a region with a retentive circulation and weak mesoscale activity (Matano et al., 2020), experienced low current speeds (<0.06 m s^{-1} Henson et al., 2022). During our study, we did not observe evidence of subsurface advection (based on high-resolution salinity and temperature profiles obtained with the gliders; Henson et al., 2022), indicating that eddy subduction was negligible. The exception was a temporary advection signal from the 16th Dec 2017 onwards, which was apparent in both the glider profiles (see also Fig. 4a) as well as in satellite data (*not shown*). However, this date was after the end of our last visit to the study site (P3C), indicating that our budgets were likely observing a quasi-1D system.

The mixed-layer pump (Gardner et al., 1995) typically occurs during the early phases of the spring bloom, during the winter-spring transition, before the onset of seasonal stratification. Periods of weak stratification that promote surface primary production are interspersed with periods of weather-driven short-term mixing, which transports the new biomass to depth (Dall'Olmo and Mork, 2014; Giering et al., 2016). In our study region, recurrent wind-driven thermal restratification events shaped the phytoplankton bloom in the region (Carvalho, pers. comm.). Yet, we observed a strengthening of the mixed layer rather than a weakening as would be required for the mixed layer pump. Furthermore, though we observed periodic restratification events throughout the cruise, potentially leaving phytoplankton biomass at depth while a new mixing layer started, we did not see active mixing below the seasonal MLD of ~70 m (Carvalho, pers. comm.). The remnant winter water (100–200 m depth; Carmack and Foster, 1975), characterised by temperature minimum, likely acted as a physical barrier for deep vertical mixing. We hence consider it unlikely that the mixed-layer pump contributed notably to the redistribution of the carbon within the mesopelagic zone.

The seasonal-lipid pump concerns the annual phenomenon of copepods, a type of zooplankton, migrating to depth for hibernation over the winter (Jónasdóttir et al., 2015). As our study was carried out during the spring, this pump was likely not applicable here.

Finally, larger zooplankton and fish are known to migrate between the surface ocean and the mesopelagic zone, and these organisms can hence redistribute organic matter in the form of biomass, excretion and egestion products (collectively termed the mesopelagic-migrant pump) (Steinberg and Landry, 2017). Often, migration is synchronised following the day-night pattern, and carbon export via this diel vertical migration can be equivalent to 40% of total carbon export (Brierley, 2014). However, during our study, we did not observe signs of synchronous diel vertical migration in total biomass or acoustic backscatter, and only a few individual groups appeared at consistently higher biomass at depth during the day (the copepod *Metridia* spp., salps, fish and decapods). Other migration patterns include reverse synchronous diel vertical migration, when populations migrate to the surface ocean during the day (e.g. Ohman et al., 1983), sporadic synchronous vertical migration, when populations do not migrate every day (e.g. Darnis et al., 2017), and asynchronous migration, when individuals of the same group migrate independently (e.g. Cottier et al., 2006). A lack of classical diel vertical migration has been observed during the main season of primary production in high-latitude regions (e.g. Darnis et al., 2017), and migration behaviour may be adapted depending on the environmental conditions (Bandara et al., 2021; Cresswell et al., 2009). Hence, the vertical transfer during our study may have occurred via a mix of migration patterns that concealed the extent of overall migration.

We can explore whether migration could have transported sufficient carbon to depth by carrying out a rough calculation. Mesozooplankton (>330 μm) and micronekton (>4 mm) biomass was ~15,000 mg C m^{-2} (0–62 m depth) and 300 mg C m^{-2} (0–250 m depth), respectively. The deficit between POC flux supply and stock accumulation in the lower mesopelagic during P3A and P3B (74 and 164 mg C m^{-2} d^{-1}, respectively; Fig. 9) was hence equivalent to ~0.5–1.1% of the mesozooplankton biomass and 25–55% of the micronekton biomass. Though the amount that mesozooplankton ingest daily ranges from <1 to 150% of their body weight (e.g. Castellani et al., 2008; Cowles and Fessenden, 1995; Mayor et al., 2006, only a small fraction of the ingested material would be carried to depth before egestion there. For micronekton, this 'gut flux' has been estimated to be 40% of the respired carbon (see refs in Hernández-León et al., 2019), and we assume the same percentage for mesozooplankton here. Respiration and excretion by common vertical migrators (subtropical North Atlantic) are, respectively, 10% (range 3–22%) and 4% (range 1–10%) (Steinberg et al., 2000). Gut flux by mesozooplankton and micronekton could hence have been ~600 mg C m^{-2} d^{-1} (range 180–1320 mg C m^{-2} d^{-1}) and ~12 mg C m^{-2} d^{-1} (range 3.6–26.4 mg C m^{-2} d^{-1}), provided the entire community migrated. In addition, migrators would have released additional carbon through excretion, which could have fuelled prokaryotic biomass production via the microbial loop. Assuming migrators spent 12 h at depth, an additional 300 mg C m^{-2} d^{-1} (range 75–750 mg C m^{-2} d^{-1}) and 6 mg C m^{-2} d^{-1} (range 1.5–15 mg C m^{-2} d^{-1}) may have been excreted by mesozooplankton and micronekton, respectively. When combining the mid-estimates of both gut flux and excretion, 8–18% of the surface mesozooplankton community or 4–9 times the surface micronekton community would have had to migrate to transport sufficient carbon to the lower mesopelagic zone to balance our lower mesopelagic carbon budgets. Asynchronous vertical migration hence remains as a possible transfer mechanism.

In conclusion, we cannot conclusively explain the vertical transfer of particulate organic matter observed here with any of the mechanisms known to us. Note though, that the budget deficit in the lower mesopelagic zone was relatively small compared to the excess in the upper mesopelagic zone. Overall, the vertical imbalance in mesopelagic carbon budgets remains an exciting knowledge gap that is waiting to be explained.

Author statement

Giering: Conceptualization, Methodology, Formal analysis, Investigation, Validation, Visualization, Writing **Sanders:** Conceptualization, Funding acquisition, Investigation, Writing, **Blackbird:** Sample analysis **Briggs:** Methodology, Investigation, Validation, Writing **Carvalho:** Methodology, Investigation, Validation, Writing **East:** Sample analysis, Data curation, Investigation **Espinola:** Sample analysis, Investigation **Henson:** Conceptualization, Writing **Kiriakoulakis:** Sample collection **Iversen:** Sample collection, Writing **Lampitt:** Conceptualization, Sample collection **Pabortsava:** Sample analysis **Pebody:** Sample analysis **Peele:** Sample analysis **Preece:** Sample analysis **Saw:** Engineering, Methodology **Villa-Alfageme**: Investigation, Writing **Wolff:** Investigation, Writing.

Funding sources

This work was funded by the Natural Environment Research Council through the COMICS project (Controls over Ocean Mesopelagic Interior Carbon Storage; NE/M020835/1). Deployment of two gliders and associated analysis was funded by European Research Council Consolidator grant (GOCART, agreement number 724416). Technical assistance with glider deployments was provided by Sea Technology Services (South Africa) and Marine Autonomous Robotic Systems (NOC). A third glider was provided by South Africa's Department of Science and Innovation (DST/CON0182/2017) and the National Research Foundation (SANAP: SNA170522231782). MVA was supported by PAIDI-Junta de Andalucía funded project TRACECARBON-P20_01217.

Declaration of competing interest

The authors declare that they have no known competing financial interests or personal relationships that could have appeared to influence the work reported in this paper.

Data availability

Data will be made available on request.

Acknowledgements

We thank the captain and crew of the RSS Discovery during DY086 as well as the South Atlantic Environmental Research Institute (SAERI) for their help during mobilisation. We thank all scientists within the COMICS programme for comments and discussion. Finally, we thank the editors and reviewers for their constructive feedback.

Appendix A. Supplementary data

Supplementary data to this article can be found online at https://doi.org/10.1016/j.dsr2.2023.105277.

References

Henson, S., Briggs, N., Carvalho, F., Manno, C., Mignot, A., Thomalla, S., 2022. Seasonal Variability in Biological Carbon Pump Efficiency in the Northern Scotia Sea. Southern Ocean, This issue.

Preece, C., Blackbird, S., Kiriakoulakis, K., Tarling, G.A., Cook, K., Mayor, D.J., Atherden, F., Giering, S.L.C., Stowasser, G., Wolff, G.A., 2022. Insights into the Fate of Particulate Organic Matter in the Mesopelagic Zone, Scotia Sea, Southern Atlantic Ocean. In preparation.

Rayne, R.R.-P., Giering, S.L.C., Hartmann, M., Sanders, R., Evans, C., 2022. Insights into Prokaryotic Carbon and Energy Limitation in the Epi and Mesopelagic from Leucine Supply and Assimilation Efficiency during a POC Export Event. This issue.

Villa-Alfageme, M., Briggs, N., Ceballos-Romero, E., de Soto, F., Manno, C., Giering, S.L. C., 2022. Seasonal Variations of Sinking Velocities in Austral Diatom Blooms: Lessons Learned from COMICS I. This issue.

Ainsworth, J., Poulton, A.J., Lohan, M.C., Stinchcombe, M.C., Lough, A.J.M., Moore, C. M., 2023. Iron cycling during the decline of a South Georgia diatom bloom. Deep Sea Res. Part II Top. Stud. Oceanogr. 208, 105269 https://doi.org/10.1016/j.dsr2.2023.105269.

Arteaga, L., Haëntjens, N., Boss, E., Johnson, K.S., Sarmiento, J.L., 2018. Assessment of export efficiency equations in the Southern Ocean applied to satellite-based net primary production. J. Geophys. Res.: Oceans 123, 2945–2964. https://doi.org/10.1002/2018JC013787.

Atkinson, A., Whitehouse, M.J., Priddle, J., Cripps, G.C., Ward, P., Brandon, M.A., 2001. South Georgia, Antarctica: a productive, cold water, pelagic ecosystem. Mar. Ecol. Prog. Ser. 216, 279–308. https://doi.org/10.3354/meps216279.

Baker, C.A., Estapa, M.L., Iversen, M., Lampitt, R., Buesseler, K., 2020. Are all sediment traps created equal? An intercomparison study of carbon export methodologies at the PAP-SO site. Prog. Oceanogr. 184, 102317 https://doi.org/10.1016/j.pocean.2020.102317.

Baltar, F., Aristegui, J., Gasol, J.M., Sintes, E., Herndl, G.J., 2009. Evidence of prokaryotic metabolism on suspended particulate organic matter in the dark waters of the subtropical North Atlantic. Limnol. Oceanogr. 54, 182–193.

Bandara, K., Varpe, Ø., Wijewardene, L., Tverberg, V., Eiane, K., 2021. Two hundred years of zooplankton vertical migration research. Biol. Rev. 96, 1547–1589. https://doi.org/10.1111/brv.12715.

Bannon, C.C., Campbell, D.A., 2017. Sinking towards destiny: high throughput measurement of phytoplankton sinking rates through time-resolved fluorescence plate spectroscopy. PLoS One 12, e0185166. https://doi.org/10.1371/journal.pone.0185166.

Benner, R., Amon, R.M.W., 2015. The size-reactivity continuum of major bioelements in the ocean. Ann. Rev. Mar. Sci 7, 185–205. https://doi.org/10.1146/annurev-marine-010213-135126.

Borrione, I., Schlitzer, R., 2013. Distribution and recurrence of phytoplankton blooms around South Georgia, Southern Ocean. Biogeosciences 10, 217–231. https://doi.org/10.5194/bg-10-217-2013.

Boyd, P.W., Claustre, H., Levy, M., Siegel, D.A., Weber, T., 2019. Multi-faceted particle pumps drive carbon sequestration in the ocean. Nature 568, 327–335. https://doi.org/10.1038/s41586-019-1098-2.

Boyd, P.W., Sherry, N.D., Berges, J.A., Bishop, J.K.B., Calvert, S.E., Charette, M.a., Giovannoni, S.J., Goldblatt, R., Harrison, P.J., Moran, S.B., Roy, S., Soon, M., Strom, S., Thibault, D., Vergin, K.L., Whitney, F.a., Wong, C.S., 1999. Transformations of biogenic particulates from the pelagic to the deep ocean realm. Deep Sea Research II 46, 2761–2792. https://doi.org/10.1016/S0967-0645(99)00083-1.

Brierley, A.S., 2014. Diel vertical migration. Curr. Biol. 24, R1074–R1076. https://doi.org/10.1016/j.cub.2014.08.054.

Briggs, N., Dall'Olmo, G., Claustre, H., 2020. Major role of particle fragmentation in regulating biological sequestration of CO 2 by the oceans. Science 367, 791–793. https://doi.org/10.1126/science.aay1790.

Briggs, N., Perry, M.J., Cetinić, I., Lee, C., D'Asaro, E., Gray, A.M., Rehm, E., 2011. High-resolution observations of aggregate flux during a sub-polar North Atlantic spring bloom. Deep Sea Res. Oceanogr. Res. Pap. 58, 1031–1039. https://doi.org/10.1016/j.dsr.2011.07.007.

Buesseler, K.O., Boyd, P.W., 2009. Shedding light on processes that control particle export and flux attenuation in the twilight zone of the open ocean. Limnol. Oceanogr. 54, 1210–1232. https://doi.org/10.4319/lo.2009.54.4.1210.

Briggs, Nathan T., Slade, Wayne H., Boss, Emmanuel, Perry, Mary Jane, 2013. Method for estimating mean particle size from high-frequency fluctuations in beam attenuation or scattering measurements. Appl. Opt. 52, 6710–6725. https://doi.org/10.1364/AO.52.006710.

Buesseler, K.O., Antia, A.N., Chen, M., Fowler, S.W., Gardner, W.D., Gustafsson, O., Harada, K., Michaels, A.F., van der Loeff, M., Sarin, M., Loeff, M.R.V.D., Sarin, M., 2007. An assessment of the use of sediment traps for estimating upper ocean particle fluxes. J. Mar. Res. 65, 345–416.

Buesseler, K.O., Boyd, P.W., Black, E.E., Siegel, D.A., 2020. Metrics that matter for assessing the ocean biological carbon pump. Proc. Natl. Acad. Sci. USA 117, 9679–9687. https://doi.org/10.1073/pnas.1918114117.

Burd, A.B., Hansell, D.a., Steinberg, D.K., Anderson, T.R., Arístegui, J., Baltar, F., Beaupré, S.R., Buesseler, K.O., DeHairs, F., Jackson, G.a., Kadko, D.C., Koppelmann, R., Lampitt, R.S., Nagata, T., Reinthaler, T., Robinson, C., Robison, B. H., Tamburini, C., Tanaka, T., 2010. Assessing the apparent imbalance between geochemical and biochemical indicators of meso- and bathypelagic biological activity: what the @$#! is wrong with present calculations of carbon budgets? Deep Sea Research II 57, 1557–1571. https://doi.org/10.1016/j.dsr2.2010.02.022.

Burd, A.B., Jackson, G.A., 2009. Particle aggregation. Ann. Rev. Mar. Sci 1, 65–90. https://doi.org/10.1146/annurev.marine.010908.163904.

Calleja, M.Ll, Al-Otaibi, N., Morán, X.A.G., 2019. Dissolved organic carbon contribution to oxygen respiration in the central Red Sea. Sci. Rep. 9, 4690. https://doi.org/10.1038/s41598-019-40753-w.

Carmack, E.C., Foster, T.D., 1975. On the flow of water out of the Weddell Sea. Deep Sea Research and Oceanographic Abstracts 22, 711–724. https://doi.org/10.1016/0011-7471(75)90077-7.

Castellani, C., Irigoien, X., Mayor, D.J., Harris, R.P., Wilson, D., 2008. Feeding of Calanus finmarchicus and oithona similis on the microplankton assemblage in the irminger sea, North Atlantic. J. Plankton Res. 30, 1095–1116. https://doi.org/10.1093/plankt/fbn074.

Cetinić, I., Perry, M.J., Briggs, N.T., Kallin, E., D'Asaro, E.A., Lee, C.M., 2012. Particulate organic carbon and inherent optical properties during 2008 North Atlantic Bloom Experiment. J. Geophys. Res.: Oceans 117. https://doi.org/10.1029/2011JC007771n/a-.

Collins, J.R., Edwards, B.R., Thamatrakoln, K., Ossolinski, J.E., DiTullio, G.R., Bidle, K. D., Doney, S.C., Van Mooy, B.A.S., 2015. The multiple fates of sinking particles in the North Atlantic Ocean. Global Biogeochem. Cycles 29, 1471–1494. https://doi.org/10.1002/2014GB005037.

Cottier, F.R., Tarling, G.A., Wold, A., Falk-Petersen, S., 2006. Unsynchronised and synchronised vertical migration of zooplankton in a high Arctic fjord. Limnol. Oceanogr. 51, 2586–2599. https://doi.org/10.4319/lo.2006.51.6.2586.

Cowles, T.J., Fessenden, L.M., 1995. Copepod grazing and fine-scale distribution patterns during the Marine Light-Mixed Layers experiment. J. Geophys. Res. 100, 6677–6686.

Cresswell, K.A., Tarling, G.A., Thorpe, S.E., Burrows, M.T., Wiedenmann, J., Mangel, M., 2009. Diel vertical migration of Antarctic krill (Euphausia superba) is flexible during advection across the Scotia Sea. J. Plankton Res. 31, 1265–1281. https://doi.org/10.1093/plankt/fbp062.

Dall'Olmo, G., Mork, K.A., 2014. Carbon export by small particles in the Norwegian Sea. Geophys. Res. Lett. 41, 2921–2927. https://doi.org/10.1002/2014GL059244.

Darnis, G., Hobbs, L., Geoffroy, M., Grenvald, J.C., Renaud, P.E., Berge, J., Cottier, F., Kristiansen, S., Daase, M., E Søreide, J., Wold, A., Morata, N., Gabrielsen, T., 2017. From polar night to midnight sun: diel vertical migration, metabolism and biogeochemical role of zooplankton in a high Arctic fjord (Kongsfjorden, Svalbard). Limnol. Oceanogr. 62, 1586–1605. https://doi.org/10.1002/lno.10519.

DeLong, E., Preston, C., Mincer, T., Rich, V., 2006. Community genomics among stratified microbial assemblages in the ocean's interior. Science 311, 496–503.
Gardner, W.D., Chung, S.P., Richardson, M.J., Walsh, I.D., 1995. The oceanic mixed-layer pump. Deep Sea Res. Part II Top. Stud. Oceanogr. 42, 757–775. https://doi.org/10.1016/0967-0645(95)00037-Q.
Giering, S.L.C., Evans, C., 2022. Overestimation of prokaryotic production by leucine incorporation—and how to avoid it. Limnol. Oceanogr. 67, 726–738. https://doi.org/10.1002/lno.12032.
Giering, S.L.C., Hosking, B., Briggs, N., Iversen, M.H., 2020. The interpretation of particle size, shape, and carbon flux of marine particle images is strongly affected by the choice of particle detection algorithm. Front. Mar. Sci. 7, 564. https://doi.org/10.3389/fmars.2020.00564.
Giering, S.L.C., Humphreys, M.P., 2018. Biological pump. In: White, W. (Ed.), Encyclopedia of Geochemistry. Springer Berlin Heidelberg. https://doi.org/10.1007/978-3-319-39193-9_154-1.
Giering, S.L.C., Sanders, R., Lampitt, R.S., Anderson, T.R., Tamburini, C., Boutrif, M., Zubkov, M.V., Marsay, C.M., Henson, S.A., Saw, K., Cook, K., Mayor, D.J., 2014. Reconciliation of the carbon budget in the ocean's twilight zone. Nature 507, 480–483. https://doi.org/10.1038/nature13123.
Giering, S.L.C., Sanders, R., Martin, A.P., Henson, S.A., Riley, J.S., Marsay, C.M., Johns, D.G., 2017. Particle flux in the oceans: challenging the steady state assumption. Global Biogeochem. Cycles 31, 159–171. https://doi.org/10.1002/2016GB005424.
Giering, S.L.C., Sanders, R., Martin, A.P., Lindemann, C., Möller, K.O., Daniels, C.J., Mayor, D.J., St John, M.A., 2016. High export via small particles before the onset of the North Atlantic spring bloom. J. Geophys. Res.: Oceans 121, 6929–6945. https://doi.org/10.1002/2016JC012048.
Hansell, D.A., Orellana, M.V., 2021. Dissolved organic matter in the global ocean: a primer. Gels 7, 128. https://doi.org/10.3390/gels7030128.
Henson, S.A., Sanders, R., Madsen, E., 2012. Global patterns in efficiency of particulate organic carbon export and transfer to the deep ocean. Global Biogeochem. Cycles 26. https://doi.org/10.1029/2011GB004099. GB1028–GB1028.
Henson, S.A., Yool, A., Sanders, R., 2015. Variability in efficiency of particulate organic carbon export: a model study. Global Biogeochem. Cycles 29, 33–45. https://doi.org/10.1002/2014GB004965.
Hernández-León, S., Olivar, M.P., Fernández de Puelles, M.L., Bode, A., Castellón, A., López-Pérez, C., Tuset, V.M., González-Gordillo, J.I., 2019. Zooplankton and micronekton active flux across the tropical and subtropical atlantic ocean. Front. Mar. Sci. 6.
Iversen, M.H., Nowald, N., Ploug, H., Jackson, G.a., Fischer, G., 2010. High resolution profiles of vertical particulate organic matter export off Cape Blanc, Mauritania: degradation processes and ballasting effects. Deep Sea Res. Oceanogr. Res. Pap. 57, 771–784. https://doi.org/10.1016/j.dsr.2010.03.007.
Jackson, G.A., 1993. Flux feeding as a mechanism for zooplankton grazing and its implications for vertical particulate flux 1. Limnol. Oceanogr. 38, 1328–1331.
Jónasdóttir, S.H., Visser, A.W., Richardson, K., Heath, M.R., 2015. Seasonal copepod lipid pump promotes carbon sequestration in the deep North Atlantic. Proc. Natl. Acad. Sci. USA 112, 12122–12126. https://doi.org/10.1073/pnas.1512110112.
Kolber, Z.S., Prášil, O., Falkowski, P.G., 1998. Measurements of variable chlorophyll fluorescence using fast repetition rate techniques: defining methodology and experimental protocols. Biochim. Biophys. Acta Bioenerg. 1367, 88–106. https://doi.org/10.1016/S0005-2728(98)00135-2.
Kwon, E.Y., Primeau, F., Sarmiento, J.L., 2009. The impact of remineralization depth on the air-sea carbon balance. Nat. Geosci. 2, 630–635. https://doi.org/10.1038/ngeo612.
Lampitt, R.S., Boorman, B., Brown, L., Lucas, M., Salter, I., Sanders, R., Saw, K., Seeyave, S., Thomalla, S.J., Turnewitsch, R., 2008. Particle export from the euphotic zone: estimates using a novel drifting sediment trap, 234Th and new production. Deep Sea Res. Oceanogr. Res. Pap. 55, 1484–1502. https://doi.org/10.1016/j.dsr.2008.07.002.
Liu, L.L., Huang, R.X., 2012. The global subduction/obduction rates: their interannual and decadal variability. J. Clim. 25, 1096–1115. https://doi.org/10.1175/2011JCLI4228.1.
MacIntyre, S., Alldredge, A.L., Gotschalk, C.C., 1995. Accumulation of marines now at density discontinuities in the water column. Limnol. Oceanogr. 40, 449–468. https://doi.org/10.4319/lo.1995.40.3.0449.
Manno, C., Stowasser, G., Enderlein, P., Fielding, S., Tarling, G.A., 2015. The contribution of zooplankton faecal pellets to deep-carbon transport in the Scotia Sea (Southern Ocean). Biogeosciences 12, 1955–1965. https://doi.org/10.5194/bg-12-1955-2015.
Martin, J.H., Knauer, G.A., Karl, D.M., Broenkow, W.W., 1987. VERTEX: carbon cycling in the northeast Pacific. Deep Sea Research Part A. Oceanographic Research Papers 34, 267–285. https://doi.org/10.1016/0198-0149(87)90086-0.
Martiny, A.C., Vrugt, J.A., Lomas, M.W., 2014. Concentrations and ratios of particulate organic carbon, nitrogen, and phosphorus in the global ocean. Sci. Data 1, 140048. https://doi.org/10.1038/sdata.2014.48.
Matano, R.P., Combes, V., Young, E.F., Meredith, M.P., 2020. Modeling the impact of ocean circulation on chlorophyll blooms around South Georgia, Southern Ocean. J. Geophys. Res.: Oceans 125, e2020JC016391. https://doi.org/10.1029/2020JC016391.
Mayor, D.J., Anderson, T.R., Irigoien, X., Harris, R., 2006. Feeding and reproduction of Calanus finmarchicus during non-bloom conditions in the Irminger Sea. J. Plankton Res. 28, 1167–1179. https://doi.org/10.1093/plankt/fbl047.
Meredith, M.P., Watkins, J.L., Murphy, E.J., Ward, P., Bone, D.G., Thorpe, S.E., Grant, S.A., Ladkin, R.S., 2003. Southern ACC Front to the northeast of South Georgia: pathways, characteristics, and fluxes. J. Geophys. Res.: Oceans 108. https://doi.org/10.1029/2001JC001227.
Mignot, A., Ferrari, R., Claustre, H., 2018. Floats with bio-optical sensors reveal what processes trigger the North Atlantic bloom. Nat. Commun. 9, 190. https://doi.org/10.1038/s41467-017-02143-6.
Mikko, V., 2022. ggOceanMaps: Plot Data on Oceanographic Maps Using "ggplot2.
Moore, J., Villareal, T., 1996. Buoyancy and growth characteristics of three positively buoyant marine diatoms. Mar. Ecol. Prog. Ser. 132, 203–213. https://doi.org/10.3354/meps132203.
Mouw, C.B., Barnett, A., McKinley, G.A., Gloege, L., Pilcher, D., 2016. Phytoplankton size impact on export flux in the global ocean. Global Biogeochem. Cycles 30, 1542–1562. https://doi.org/10.1002/2015GB005355.
Ohman, M.D., Frost, B.W., Cohen, E.B., 1983. Reverse diel vertical migration: an escape from invertebrate predators. Science 220, 1404–1407. https://doi.org/10.1126/science.220.4604.1404.
Owens, S.A., Pike, S., Buesseler, K.O., 2015. Thorium-234 as a tracer of particle dynamics and upper ocean export in the Atlantic Ocean. Deep Sea Res. Part II Top. Stud. Oceanogr. 116, 42–59. https://doi.org/10.1016/j.dsr2.2014.11.010.
Parekh, P., Dutkiewicz, S., Follows, M.J., Ito, T., 2006. Atmospheric carbon dioxide in a less dusty world. Geophys. Res. Lett. 33, 2–5. https://doi.org/10.1029/2005GL025098.
Reinthaler, T., van Aken, H.M., Veth, C., Williams, P. leB., Aristegui, J., Robinson, C., Lebaron, P., Herndl, G.J., 2006. Prokaryotic respiration and production in the meso- and bathypelagic realm of the eastern and western North Atlantic basin. Limnol. Oceanogr. 51, 1262–1273.
Riley, J.S., Sanders, R., Marsay, C., Le Moigne, F.A.C., Achterberg, E.P., Poulton, A.J., 2012. The relative contribution of fast and slow sinking particles to ocean carbon export. Global Biogeochem. Cycles 26. https://doi.org/10.1029/2011GB004085. GB1026–GB1026.
Sanders, R.J., Henson, S.A., Martin, A.P., Anderson, T.R., Bernardello, R., Enderlein, P., Fielding, S., Giering, S.L.C., Hartmann, M., Iversen, M., Khatiwala, S., Lam, P., Lampitt, R., Mayor, D.J., Moore, M.C., Murphy, E., Painter, S.C., Poulton, A.J., Saw, K., Stowasser, G., Tarling, G.A., Torres-Valdes, S., Trimmer, M., Wolff, G.A., Yool, A., Zubkov, M., 2016. Controls over Ocean Mesopelagic interior carbon storage (COMICS): fieldwork, synthesis, and modeling efforts. Front. Mar. Sci. 3, 1–7. https://doi.org/10.3389/fmars.2016.00136.
Santana-Falcón, Y., Álvarez-Salgado, X.A., Pérez-Hernández, M.D., Hernández-Guerra, A., Mason, E., Arístegui, J., 2017. Organic carbon budget for the eastern boundary of the North Atlantic subtropical gyre: major role of DOC in mesopelagic respiration. Sci. Rep. 7, 10129 https://doi.org/10.1038/s41598-017-10974-y.
Steinberg, D.K., Carlson, C.A., Bates, N.R., Goldthwait, S.a., Madin, L.P., Michaels, A.F., 2000. Zooplankton vertical migration and the active transport of dissolved organic and inorganic carbon in the Sargasso Sea. Deep Sea Res. Oceanogr. Res. Pap. 47, 137–158. https://doi.org/10.1016/S0967-0637(99)00052-7.
Steinberg, D.K., Landry, M.R., 2017. Zooplankton and the ocean carbon cycle. Ann. Rev. Mar. Sci 9, 413–444. https://doi.org/10.1146/annurev-marine-010814-015924.
Steinberg, D.K., Mooy, B.A.S.V., Buesseler, K.O., Boyd, P.W., Kobari, T., Karl, D.M., 2008. Bacterial vs zooplankton control of sinking particle flux in the ocean's twilight zone. Limnol. Oceanogr. 53, 1327–1338.
Stemmann, L., Jackson, G.A., Gorsky, G., 2004. A vertical model of particle size distributions and fluxes in the midwater column that includes biological and physical processes—Part II: application to a three year survey in the NW Mediterranean Sea. Deep Sea Res. Oceanogr. Res. Pap. 51, 885–908. https://doi.org/10.1016/j.dsr.2004.03.002.
Turner, J.T., 2015. Zooplankton fecal pellets, marine snow, phytodetritus and the ocean's biological pump. Prog. Oceanogr. 130, 205–248. https://doi.org/10.1016/j.pocean.2014.08.005.
Uchimiya, M., Fukuda, H., Wakita, M., Kitamura, M., Kawakami, H., Honda, M.C., Ogawa, H., Nagata, T., 2018. Balancing organic carbon supply and consumption in the ocean's interior: evidence from repeated biogeochemical observations conducted in the subarctic and subtropical western North Pacific. Limnol. Oceanogr. 63, 2015–2027. https://doi.org/10.1002/lno.10821.
Venables, H., Meredith, M.P., Atkinson, A., Ward, P., 2012. Fronts and habitat zones in the Scotia Sea. Deep-Sea Res. Part II Top. Stud. Oceanogr. 59–60, 14–24. https://doi.org/10.1016/j.dsr2.2011.08.012.
Volk, T., Hoffert, M.I., 1985. The carbon cycle and atmospheric CO2: natural variations archean to present. In: Geophysical Monograph Series, Geophysical Monograph Series. American Geophysical Union, Washington, D. C. https://doi.org/10.1029/GM032.